INSPYRE
Investigations Supporting MOX Fuel Licensing in ESNII Prototype Reactors

EERA JPNM
JOINT PROGRAMME ON NUCLEAR MATERIALS

D7.5 – Fuel performance simulations of ESNII prototypes: Results on the MYRRHA case study

A. Magni (ENEA, POLIMI), M. Bertolus, M. Lainet, V. Marelle, B. Michel (CEA), A. Schubert, P. Van Uffelen (JRC-Ka), L. Luzzi, D. Pizzocri (POLIMI), B. Boer, S. Lemehov (SCK.CEN), A. Del Nevo (ENEA)

Version 1 – 02/12/2022

The INSPYRE project has received funding from the EURATOM research and training programme 2014-2018 under Grant Agreement No 754329.

Document type	Deliverable
Document number	D7.5 version 1
Document title	Fuel performance simulations of ESNII prototypes: Results on the MYRRHA case study
Authors	A. Magni (ENEA, POLIMI), M. Bertolus, M. Lainet, V. Marelle, B. Michel (CEA), A. Schubert, P. Van Uffelen (JRC-Ka), L. Luzzi, D. Pizzocri (POLIMI), B. Boer, S. Lemehov (SCK.CEN), A. Del Nevo (ENEA)
Release date	02/12/2022
Contributing partners	ENEA, CEA, JRC, POLIMI, SCK.CEN
Dissemination level	Public

Version	Short description	Main author	WP leader	Coordinator
1	First release	A. Magni (ENEA, POLIMI) 22/11/2022	L. Luzzi (POLIMI) 22/11/2022	M. Bertolus (CEA) 02/12/2022

SUMMARY

Nominal and transient conditions of the ESNII prototypes were investigated in the INSPYRE Project using the European fuel performance codes GERMINAL, MACROS and TRANSURANUS. This Deliverable presents the results of the simulations of the MYRRHA case study: MYRRHA nominal irradiation conditions and the occurrence of a beam power jump (over-power) transient at the beginning and end of life of the fuel pin in reactor. Besides the application of the reference ("pre-INSPYRE") code versions, the activity involves the evaluation of the impact of the improved models of MOX fuel properties developed in INSPYRE and implemented in the three fuel performance codes. These modelling advances concern the thermal properties (thermal conductivity, melting temperature), mechanical properties (thermal expansion, Young's modulus) and the mechanistic treatment of fission gas behaviour and release from MOX fuels.

The results yielded by the pre-INSPYRE and post-INSPYRE versions of the codes involved are presented and assessed in terms of evolution in time, as well as axial and radial profiles of significant quantities, both integral and local. Then, the code results are compared with the design limits set for the MYRRHA fuel pins, in particular the maximal fuel temperature admitted, which prevents fuel melting, and the maximal allowed cladding plasticity that ensures the cladding integrity. The outcome is a complete compliance of the pin behaviour with the design limits, respecting adequate margins even in the case of the hottest fuel pin and in the case of beam power jump transients.

CONTENT

GLOSSARY

ADS	Accelerator Driven System
BPJ	Beam Power Jump
DIN	Deutsches Institut für Normung
ECR	Electron-Cyclotron Resonance
EFPD	Effective Full Power Days
ESNII	European Sustainable Nuclear Industrial Initiative
FA	Fuel Assembly
FPC	Fuel Performance Code
FR	Fast Reactor
GFR	Gas Fast Reactor
HM	Heavy Metal
INSPYRE	Investigations Supporting MOX Fuel Licensing for ESNII Prototype Reactors
JPNM	Joint Programme on Nuclear Materials
LBE	Lead-Bismuth Eutectic
LFR	Lead Fast Reactor
LINAC	LINear Accelerator
LWR	Light Water Reactor
MOX	Mixed-OXide
MYRRHA	Multi-purpose hYbrid Research Reactor for High-tech Applications
NEA	Nuclear Energy Agency
O/M	Oxygen-to-Metal ratio
R&D	Research and Development
SFR	Sodium Fast Reactor
TOP	Transient Over-Power
YSZ	Yttria-Stabilised Zirconia

1 INTRODUCTION

The Generation IV International Forum (GIF) aims at introducing a new generation of innovative and inherently safe nuclear reactors [1]. In this context, the European Sustainable Nuclear Industrial Initiative (ESNII) program was launched in 2010 to foster the development of four fast neutron spectrum facilities and demonstrators [2]:

- the sodium fast reactor (SFR) ASTRID [3],
- the lead fast reactor (LFR) ALFRED [4],
- the MYRRHA ADS combining a lead-bismuth eutectic (LBE) cooled fast reactor and an accelerator [5],
- the gas fast reactor (GFR) ALLEGRO [6], [7].

The MYRRHA facility under development at SCK.CEN has gained an important role in the development path leading to a dedicated Accelerator-Driven System (ADS), considering the recent growing interest in ultimate radioactive waste management, proliferation resistance and sustainability improvement by better use of fuel resources [8]. It aims at demonstrating the accelerator-driven system concept and to operate as a flexible Generation IV irradiation facility for R&D purposes.

Assessing the thermal-mechanical behaviour of fuel pins for ESNII systems is key for the reactor design due to the extremely demanding operating conditions characterizing fast reactors (high temperatures, high fast neutron fluence, chemically aggressive coolants) [9]. Fuel performance codes (FPCs) are typically used for this purpose [10], allowing one to account for the interrelationships between the numerous phenomena affecting the fuel pin under irradiation [11], [12]. Improving the predictive capabilities of FPCs related to materials and operating conditions of ESNII reactor systems is one of the objectives of the INSPYRE H2020 European Project [13].

This Deliverable presents a pin performance assessment of the MYRRHA reactor according to the pin and reactor specifications, and to design limits provided by SCK CEN (MYRRHA design “Revision 1.6” configuration [14]) in the INSPYRE Project. In particular, the compliance with the upper limit for the fuel maximal temperature, which aims at avoiding failures due to fuel melting, and the maximum cladding plasticity allowed, which ensures the cladding integrity throughout the nominal irradiation and during transients.

The simulation activities on the MYRRHA case study were performed using three European fuel performance codes (FPC):

- GERMINAL (evolution of version V2.2.5 extended to consider LBE-coolant), developed and used by CEA [15], [16]
- TRANSURANUS (versions v1m1j20 and v1m5j20) developed and used by JRC-Karlsruhe, POLIMI and ENEA, [17], [18]
- MACROS, developed and used by SCK.CEN [19], [20].

Three representative pins of the irradiation conditions in the MYRRHA core were identified, namely the hottest, average and coldest pins. The focus in this Deliverable is the performance of the hottest pin, since it experiences the worst irradiation conditions. Moreover, modelling hypotheses are employed to allow for conservative evaluations of the hottest pin thermal-mechanical behaviour. The considered irradiation scenarios, besides the nominal MYRRHA irradiation history, involve Beam Power Jump (BPJ) transients (over-power) occurring at representative moments during the normal reactor operation, i.e., at beginning-of-life and end-of-life conditions. These BPJ scenarios are identified as the most critical ones for the fuel maximal temperature (margin to fuel melting) and cladding plasticity potentially

caused by fuel-cladding gap closure and consequent pellet-cladding mechanical interaction, respectively. They therefore require dedicated evaluations.

The Deliverable is structured as follows. Section 2 provides a general description of the MYRRHA irradiation facility and reactor core, the specifications of the case study considered in work and the simulation strategy with the fuel performance codes involved. The results yielded by the three codes considered on the MYRRHA nominal irradiation conditions are presented in Section 3. Section 4 focuses on the simulation and analysis of the BPJ transient scenarios, both for beginning-of-life and end-of-life conditions. The compliance with the MYRRHA design limits is also analysed in Section 4. Conclusions are drawn and future developments of this work are presented in Section 5.

2 MYRRHA PROTOTYPE, CASE STUDY SPECIFICATIONS AND CODES USED

Since 1998, the Belgian nuclear research centre SCK.CEN is designing a multi-purpose irradiation facility for research and development applications called MYRRHA (Multi-purpose hYbrid Research Reactor for High-tech Applications) [21]. It is conceived as a flexible experimental accelerator driven system to demonstrate the ADS concept itself and to study the technological feasibility of minor actinides and long-lived fission products transmutation under fast neutron irradiation [8]. This matches the R&D needs and expectations related to fast reactors of Generation IV [22]. The current application purposes of MYRRHA are to:

- demonstrate the ADS concept at a reasonable power level (more than 50 MW_{th}), scalable to an industrial demonstrator
- allow the study of the efficient transmutation of high-level nuclear waste, with particular focus on minor actinides
- be operated as a flexible fast spectrum irradiation facility allowing for materials development for Gen IV and fusion reactors
- study and produce radioisotopes for medical and industrial applications.

The MYRRHA reactor concept was selected as one of the two applicative case studies (representative of ESNII reactor conditions) of the INSPYRE Project.

2.1 Description of the MYRRHA facility

The MYRRHA reactor is designed as a pool-type, LBE-cooled fast reactor. It will be able to operate both in critical and sub-critical mode (i.e., as an ADS) [23]. As far as the material selection is concerned, the MYRRHA project team has favoured as much as possible the employment of mature or less demanding technologies in terms of R&D [24]. Following this approach, an austenitic stainless steel 15-15Ti (specifically, the DIN 1.4970 alloy annealed and cold worked) was selected as cladding.

As an accelerator driven system, the MYRRHA sub-critical core is coupled to a proton accelerator delivering its beam to a liquid LBE spallation target located in a dedicated assembly at the core centre. The optimal solution for the ADS design and performances turned out to be a 600 MeV LINAC (LINear ACcelerator) with an average proton beam current up to 4 mA [25].

Details about the design of the MYRRHA pool-type reactor can be found in references [26] and [27]. The reference for this work is the "MYRRHA Revision 1.6" design. A vertical cut of the reactor vessel showing its main internal components is represented in Figure 1 [27].

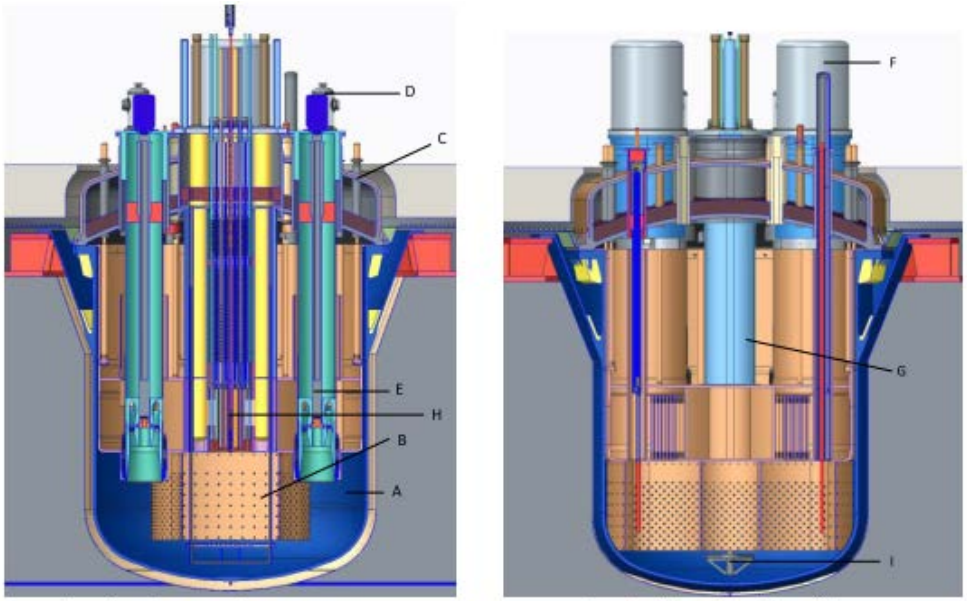

Figure 1: Vertical section of the MYRRHA reactor vessel, showing the main in-vessel components [27].

The MYRRHA core layout depends on the reactor operational mode, which can be critical or sub-critical. The sub-critical ADS configuration is the focus of the present analysis (Figure 2 – right) [28]. A schematic representation of the two possible core layouts is shown in Figure 2.

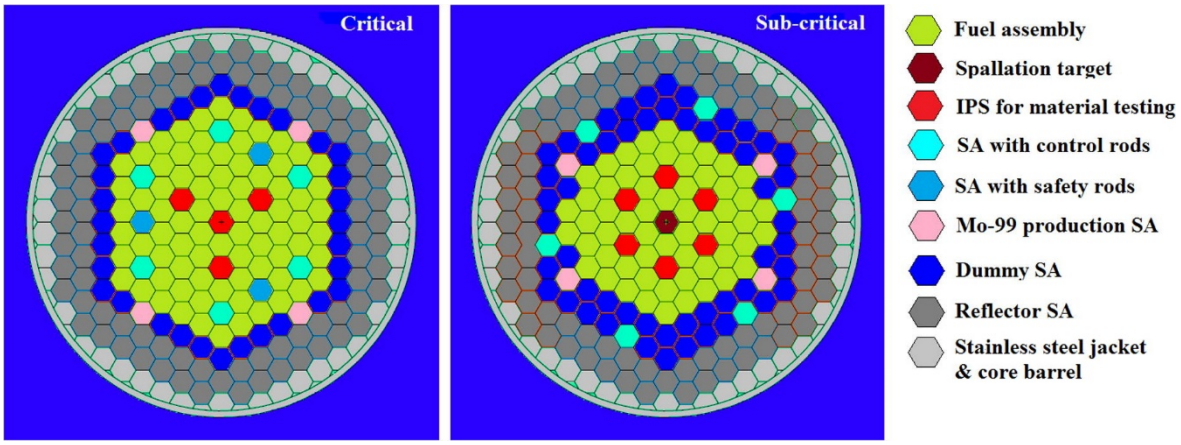

Figure 2: MYRRHA critical (left) and sub-critical (right) core layouts [29].

2.2 MYRRHA fuel assembly and element specifications

The MYRRHA fuel assembly (FA) consists in a bundle of fuel pins arranged in a triangular lattice, surrounded by a hexagonal shroud or wrapper. Each pin in a fuel bundle is equipped with helical wire-spacers wounds on the outer surface, to keep them separated from one another and guarantee their proper coolability [30].

The fuel pin consists of a cylindrical 15-15Ti stainless steel cladding (DIN 1.4970) loaded with MOX fuel pellets. Ending insulator segments in yttria-stabilised zirconia (YSZ) ceramics are included [24]. Upper

and lower plena are designed to accommodate the fission gases released by the fuel during irradiation. A larger lower plenum is envisaged to promote the gas accumulation in the colder region and thus reduce the gas pressure in the fuel pin. The design specifications of standard MYRRHA fuel pins are reported in Table 1.

Parameter	Value
Pellet outer diameter	5.42 mm
Cladding inner diameter	5.65 mm
Cladding outer diameter	6.55 mm
Active fuel length	650 mm
Upper and lower insulator segments length [a]	35 mm
Lower plenum length	580 mm
Upper plenum length [b]	60 mm
Filling gas (He) pressure	0.1 MPa
Oxygen/Metal ratio	1.97
Uranium [c]/Metal ratio	0.70
Plutonium [d]/Metal ratio	0.30
As-fabricated porosity	5%
Grain size	15 µm
[a] Above / below the active length: material made with YSZ.	
[b] Assumed that 30% of the upper plenum volume is occupied by the spring.	
[c] U isotopic composition: ^{234}U = 0.0053 wt.%, ^{235}U = 0.7114 wt.%, ^{238}U = 99.283 wt.% (assumed natural uranium isotopic composition)	
[d] Pu isotopic composition: ^{238}Pu = 2.332 wt.%, ^{239}Pu = 56.873 wt.%, ^{240}Pu = 26.997 wt.%, ^{241}Pu = 6.105 wt.%, ^{242}Pu = 7.693 wt.%	

Table 1: Main fuel pin specifications related to the MYRRHA case study considered in INSPYRE.

2.3 MYRRHA operating schedule

A typical MYRRHA operating schedule consists of 90 Effective Full Power Days (EFPD) followed by 30 days of shutdown for core reshuffling, loading and maintenance [28]. After every irradiation cycle, a core reconfiguration is foreseen: batches composed by six fuel assemblies are shuffled towards outer regions of the MYRRHA core, and fresh fuel is added close to the central spallation target, in order to compensate the reactivity loss. In this way, the final fuel burnup at the end of the driver irradiation for each fuel element is homogenized (expected to be around 70 MWd/kg_{HM} both in critical and sub-critical core configurations).

2.4 Case study description

The MYRRHA case study simulated in INSPYRE using GERMINAL, MACROS and TRANSURANUS fuel performance codes consists in 1) normal operation of MYRRHA, sub-critical (ADS) core configuration 2) a protected Transient Over-Power (TOP) scenario occurring while MYRRHA is operating in its ADS configuration.

2.4.1 Normal operating conditions simulated

According to the MYRRHA core design and irradiation strategy, exploiting the symmetry of the core, a fresh batch of fuel assemblies undergoes a 12-cycle irradiation history in the sub-critical core configuration. The batch positions are highlighted in Figure 3 – left. The fuel assemblies, re-shuffled every 90 EFPD of operation, experience different irradiation conditions during each cycle, both in terms of neutron flux and power produced (Figure 3– right).

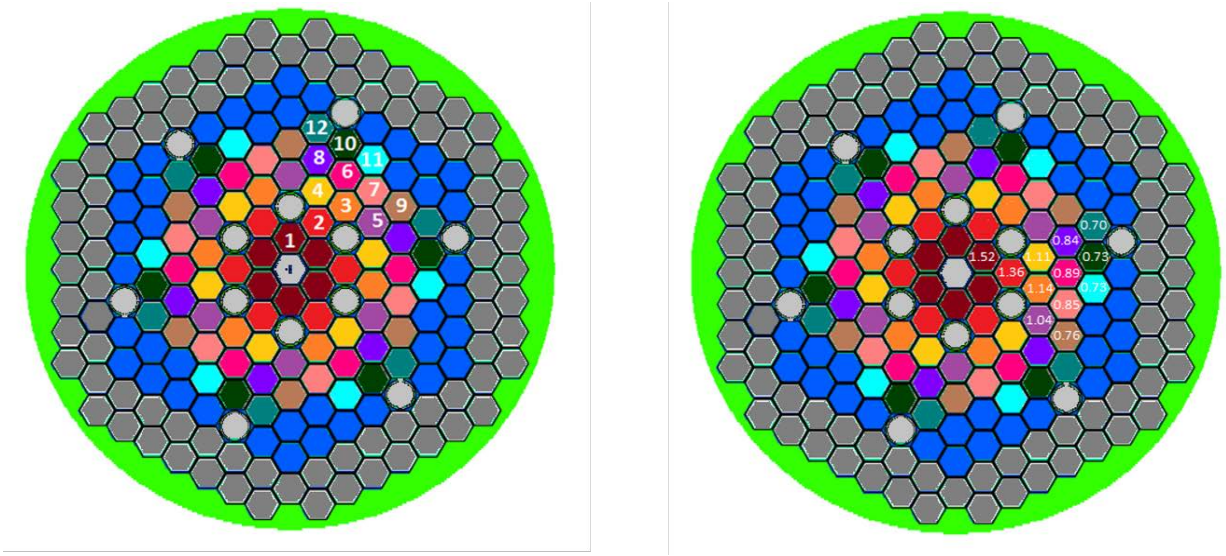

Figure 3: Batch positions (left) and power produced (in MW per FA) by each batch (right) in the sub-critical core configuration considered [28].

The irradiation and cooling conditions faced by the fuel pins within the same fuel assembly also depend on the pin position in the FA itself, which varies during the 12 cycles composing the nominal irradiation history. The actual positions of the hottest and coldest pins within the FAs are highlighted for each core position in Figure 4 for the sub-critical core configuration considered. The hottest and coldest pins in an assembly are not necessarily the same during the different irradiation cycles.

However, three (artificial) reference pin irradiation histories have been considered corresponding to the sequence of hottest, average and coldest pin locations during each irradiation cycle. This simulation strategy does not match the real irradiation conditions foreseen for the MYRRHA base-irradiation, but allows a conservative evaluation of the pin performance since in this way the hot pin simulated experiences the worst conditions throughout the 12 cycles. To move from one irradiation position to the subsequent, ramps (of discharge and re-loading) lasting 0.5 h are considered, and similarly the initial start-up and final shut-down ramps are 0.5 h long. Details about the MYRRHA nominal irradiation histories considered, in terms of linear heat rate and fast neutron flux at the axial peak power node of the three representative pins, are provided in Table 2.

The axial profiles of both pin linear power and fast neutron flux, as a function of time along the nominal irradiation history, considered in this work as inputs for the fuel performance code simulations, are kept constant during each irradiation cycle. The power produced and fast neutron flux gradually decrease towards the end of irradiation because of the reshuffling scheme applied for the MYRRHA sub-critical core (Figure 5).

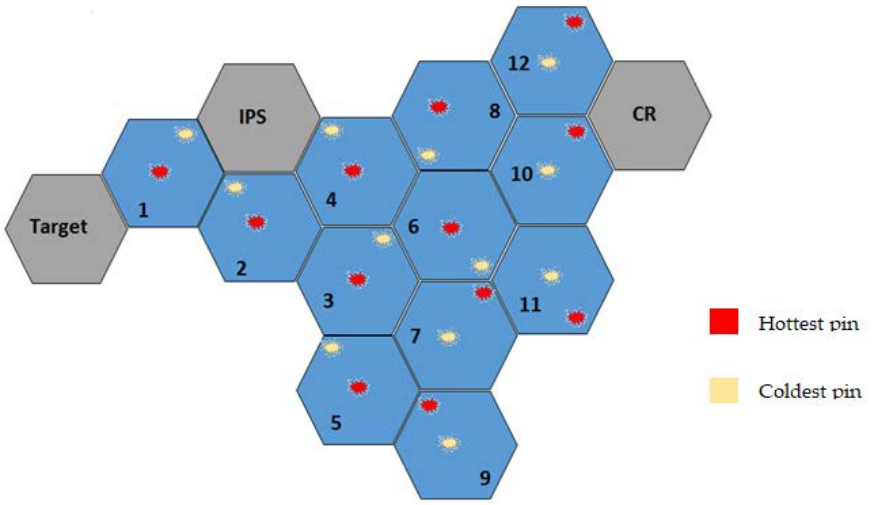

Figure 4: Positions of the hottest and coldest pins during each irradiation cycle.

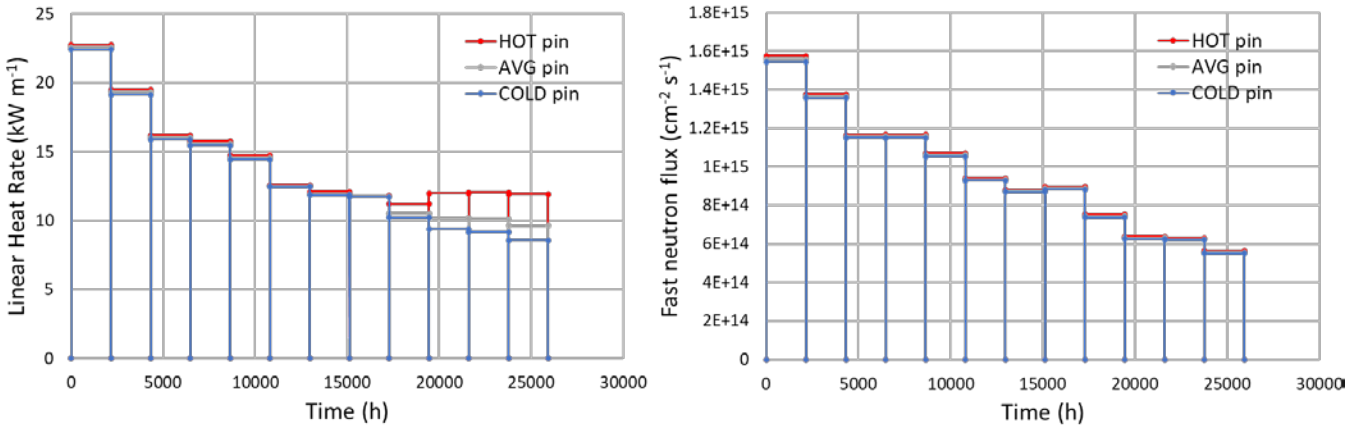

Figure 5: Evolution in time of the linear heat rate (left) and fast neutron flux (right), at the axial peak power node, for the representative hot (red curve), average (grey curve) and cold (blue curve) pins during the MYRRHA nominal irradiation schedule.

In the MYRRHA scenario defined for the INSPYRE Project, the MYRRHA thermal power is set to be at 70 MWth. The coolant – Lead-Bismuth Eutectic (LBE) – inlet temperature in the core is equal to 518 K (245 °C) and assumed to be constant during reactor operation, as well as the LBE pressure (0.6 MPa).

The LBE mass flow rates (per pin) are kept constant during irradiation and depend on the pin position in the batch in each cycle (see Figure 4). They are equal to:

- 0.48 kg s^{-1} for the inner pins
- 0.56 kg s^{-1} for the average pins
- 0.76 kg s^{-1} for the peripheral pins: this value refers to the average flow area of peripheral pins (38.33 mm^2), obtained by the weighted average between the 30 edge-pins and the 6 corner-pins flow areas.

The following correlation is adopted for the heat capacity of LBE as a function of temperature [31]:

$$c_p(J\ kg^{-1}K^{-1}) = 164.8 - 3.94\ x\ 10^{-2} \cdot T + 1.25\ x\ 10^{-5} \cdot T^2 - 4.56\ x\ 10^{5} \cdot T^{-2}$$

		Hottest pin		Average pin		Coldest pin	
# cycle	Time (h)	Linear Heat Rate (kW m^{-1})	Flux (cm^{-2} s^{-1})	Linear Heat Rate (kW m^{-1})	Flux (cm^{-2} s^{-1})	Linear Heat Rate (kW m^{-1})	Flux (cm^{-2} s^{-1})
	0	0	0	0	0	0	0
1	0.5	22.74	$1.58\cdot10^{15}$	22.61	$1.56\cdot10^{15}$	22.42	$1.54\cdot10^{15}$
	2160.5	22.74	$1.58\cdot10^{15}$	22.61	$1.56\cdot10^{15}$	22.42	$1.54\cdot10^{15}$
	2161	0	0	0	0	0	0
2	2161.5	19.51	$1.38\cdot10^{15}$	19.34	$1.37\cdot10^{15}$	19.14	$1.36\cdot10^{15}$
	4321.5	19.51	$1.38\cdot10^{15}$	19.34	$1.37\cdot10^{15}$	19.14	$1.36\cdot10^{15}$
	4322	0	0	0	0	0	0
3	4322.5	16.22	$1.1656\cdot10^{15}$	16.06	$1.1578\cdot10^{15}$	15.88	$1.149\cdot10^{15}$
	6482.5	16.22	$1.1656\cdot10^{15}$	16.06	$1.1578\cdot10^{15}$	15.88	$1.149\cdot10^{15}$
	6483	0	0	0	0	0	0
4	6483.5	15.78	$1.1662\cdot10^{15}$	15.62	$1.1582\cdot10^{15}$	15.46	$1.150\cdot10^{15}$
	8643.5	15.78	$1.1662\cdot10^{15}$	15.62	$1.1582\cdot10^{15}$	15.46	$1.150\cdot10^{15}$
	8644	0	0	0	0	0	0
5	8644.5	14.72	$1.07\cdot10^{15}$	14.59	$1.06\cdot10^{15}$	14.42	$1.05\cdot10^{15}$
	10804.5	14.72	$1.07\cdot10^{15}$	14.59	$1.06\cdot10^{15}$	14.42	$1.05\cdot10^{15}$
	10805	0	0	0	0	0	0
6	10805.5	12.60	$9.41\cdot10^{14}$	12.51	$9.34\cdot10^{14}$	12.44	$9.28\cdot10^{14}$
	12965.5	12.60	$9.41\cdot10^{14}$	12.51	$9.34\cdot10^{14}$	12.44	$9.28\cdot10^{14}$
	12966	0	0	0	0	0	0
7	12966.5	12.11	$8.805\cdot10^{14}$	11.91	$8.74\cdot10^{14}$	11.85	$8.68\cdot10^{14}$
	15126.5	12.11	$8.805\cdot10^{14}$	11.91	$8.74\cdot10^{14}$	11.85	$8.68\cdot10^{14}$
	15127	0	0	0	0	0	0
8	15127.5	11.81	$8.96\cdot10^{14}$	11.77	$8.89\cdot10^{14}$	11.71	$8.81\cdot10^{14}$
	17287.5	11.81	$8.96\cdot10^{14}$	11.77	$8.89\cdot10^{14}$	11.71	$8.81\cdot10^{14}$
	17288	0	0	0	0	0	0
9	17288.5	11.21	$7.52\cdot10^{14}$	10.53	$7.44\cdot10^{14}$	10.23	$7.38\cdot10^{14}$
	19448.5	11.21	$7.52\cdot10^{14}$	10.53	$7.44\cdot10^{14}$	10.23	$7.38\cdot10^{14}$
	19449	0	0	0	0	0	0
10	19449.5	11.98	$6.38\cdot10^{14}$	10.19	$6.32\cdot10^{14}$	9.39	$6.25\cdot10^{14}$
	21609.5	11.98	$6.38\cdot10^{14}$	10.19	$6.32\cdot10^{14}$	9.39	$6.25\cdot10^{14}$
	21610	0	0	0	0	0	0
11	21610.5	12.04	$6.30\cdot10^{14}$	10.09	$6.26\cdot10^{14}$	9.19	$6.20\cdot10^{14}$
	23770.5	12.04	$6.30\cdot10^{14}$	10.09	$6.26\cdot10^{14}$	9.19	$6.20\cdot10^{14}$
	23771	0	0	0	0	0	0
12	23771.5	11.94	$5.63\cdot10^{14}$	9.64	$5.57\cdot10^{14}$	8.58	$5.51\cdot10^{14}$
	25931.5	11.94	$5.63\cdot10^{14}$	9.64	$5.57\cdot10^{14}$	8.58	$5.51\cdot10^{14}$
end	25932	0	0	0	0	0	0

Table 2: Details about the irradiation histories for the representative hottest, average and coldest MYRRHA fuel pins: evolution in time of the linear heat rate and fast neutron flux at the axial peak power node during the 12 cycles composing the nominal operative schedule of the MYRRHA reactor.

2.4.2 Transient scenario simulated

The overpower transient scenario considered in the case study analysed in this work is a Beam Power Jump (BPJ). The initiating event for the BPJ transient is a sudden increase by 70% of the electron-cyclotron resonance (ECR) ion source, i.e., an accelerator beam trip, while the accelerator is working in nominal conditions (beam intensity: 4 mA, beam energy: 600 MeV, reactor core power: 70 MW). The

accelerator control system reacts to the overcurrent, increasing by 70% the feeding power in order to keep the beam energy constant at the operation target value. The maximum operating power is limited to 170% of the nominal value by the fault tolerance scheme implemented in the high-energy section of the accelerator. Above this threshold, the protection system of the accelerator intervenes and shuts off the feeding power.

The power of the MYRRHA ADS core also increases by 70%, due to the proportional relationship linking the proton beam current and the core power. Neglecting conservatively the effect of delayed neutrons on the power evolution, it is assumed that the power reaches its asymptotic value in a time step (duration 1 ms) and that the BPJ does not affect the axial power peaking factors. The accelerator shut-off is driven by a high-neutron flux signal. A high neutron flux signal prolonging for more than 3 seconds triggers the accelerator shut-off, and a scram time of 3 seconds is conservatively assumed. A sketch of the power trip simulated via fuel performance codes in INSPYRE is reported in Figure 6.

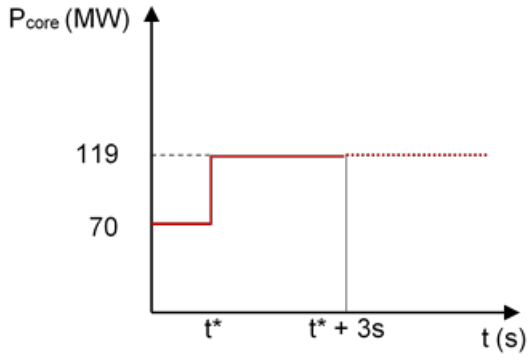

Figure 6: Sketch of MYRRHA power excursion in a BPJ scenario.

The BPJ scenario can occur at any instant of time during the MYRRHA base irradiation history (12 cycles). Three BPJ scenarios of major interest in terms of fuel pin performance are identified, i.e., at the beginning and end of the first cycle, representative of beginning-of-life conditions, and during the 12th cycle, representative of end-of-life conditions.

For what concerns the design limits, in overpower transient (TOP) scenarios pin failure can occur either by phenomena connected with fuel melting or by cladding mechanical failure (e.g., due to Pellet-Cladding Mechanical Interaction). Hence, the key safety criteria to be assessed are:

1) Melting point at 2600°C for failures caused by fuel melting in the pellet
2) Cladding plastic strain up to 0.5% for thermo-mechanical failures.

The objective of the simulations performed in INSPYRE is to assess conservatively any potential pin failure caused by a BPJ occurring in the MYRRHA subcritical core and to identify the most critical pins and irradiation cycle for both failure mechanisms.

2.5 Fuel performance codes involved

As indicated in the Introduction, the three fuel performance codes (FPCs) considered in INSPYRE are GERMINAL, TRANSURANUS and MACROS. While GERMINAL is specifically tailored to fast reactor (sodium-cooled) irradiations, TRANSURANUS is a code system primarily applied to light water reactor (LWR) conditions and extended to take into account fast neutron spectra and further specific material properties for fast reactor applications [17], [32]. MACROS is a mechanistic code that can be applied both to LWR fuels and to fast reactor (FR) systems.

Reference fuel performance simulations were performed using the "pre-INSPYRE" code versions of GERMINAL and TRANSURANUS. The reference TRANSURANUS modelling choices for properties of the MYRRHA fuel, cladding and coolant correspond to the models recommended by the code [17] to describe the behaviour under irradiation of fast reactor MOX fuels, 15-15Ti cladding steel and liquid LBE coolant [17], [32], [33] e.g., correlation for MOX fuel thermal conductivity according to Philippon-neau [34], also employed by GERMINAL. The correlations used in the MACROS and TRANSURANUS codes for the LBE thermal physical properties (e.g., boiling temperature, heat capacity, dynamic viscosity, density, thermal conductivity, enthalpy) are those recommended by the OECD/NEA Handbook on LBE and lead properties [33], [35], reported also by [36]. The same models for the properties of the liquid LBE coolant were introduced in GERMINAL for this study. In addition, the TRANSURANUS code includes the Ushakov et al. correlation [37] for the LBE turbulent heat transfer coefficient.

The "post-INSPYRE" versions of the three codes were also used for the simulations, to test the sensitivity of the MYRRHA fuel pin performance to the novel modelling options. Their implementation in the GERMINAL, MACROS and TRANSURANUS codes and the corresponding code versions is described in detail in Deliverable D7.2 [18]. In summary,

- The GERMINAL and TRANSURANUS codes were improved by integrating:
  - New correlations for the thermal conductivity and melting temperature of MOX fuels [38], [39]
  - New correlations for the thermal expansion and Young's modulus of MOX fuels [40]
  - The physics-based description of fission gas behaviour and release in MOX fuel pellets, implemented in the SCIANTIX inert gas behaviour module coupled to the FPCs [41].
- The MACROS code was extended by the implementation of the new correlations for the thermal expansion and Young's modulus of MOX fuels [40].

2.6 Global linear heat rate evolution

The first step of the study is the simulation of the entire irradiation history of the normal operating conditions and of the BPJ transients. The linear heat evolution used by the three codes is given in Figure 7, for a BPJ occurring at the end of cycle 1 (left) and at the end of cycle 12 (right). Figure 7 shows that the three codes are aligned on the same irradiation conditions set via input files. This is the fundamental basis allowing the proper comparison of the code results.

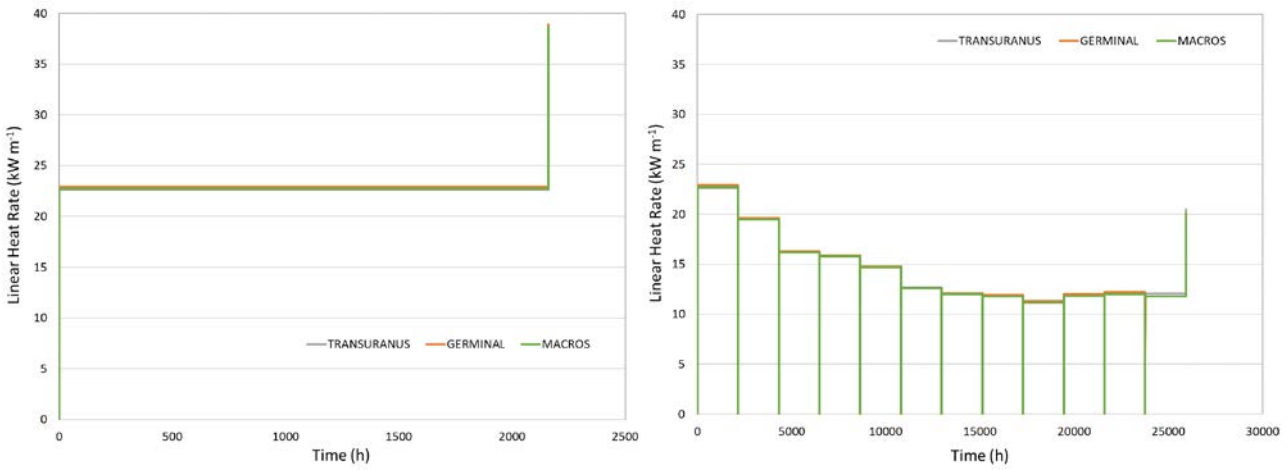

Figure 7: Linear heat evolution at the peak power node of the MYRRHA hottest pin as used by the TRANSURANUS, GERMINAL and MACROS codes, including the two transient irradiation scenarios selected: BPJ at the end of cycle 1 (left) and BPJ at the end of cycle 12 (right).

3 RESULTS OF THE SIMULATION OF MYRRHA FUEL PIN PERFORMANCE IN NORMAL OPERATION CONDITIONS

This Section presents the results of the simulation of the thermal-mechanical performance of the MYRRHA hottest fuel pin under nominal irradiation conditions performed using the GERMINAL, MACROS and TRANSURANUS fuel performance codes. The simulation results encompass axial profiles, radial profiles and evolutions in time, at both cycles 1 and 12 of the MYRRHA nominal driver fuel irradiation.

3.1 First cycle of nominal irradiation

The simulated evolution of the peak fuel burnup (at the peak power node) during the 12 irradiation cycles is reported in Figure 8. The final peak burnups reached by the fuel yielded by the various codes are similar: 72.8 GWd t_{HM}^{-1} (lower bound), 74.6 GWd t_{HM}^{-1} and 78.5 GWd t_{HM}^{-1} (upper bound) for MACROS, TRANSURANUS and GERMINAL, respectively. The small differences are due to the different burnup modules included in the codes and to the different fissile heavy metal nuclides accounted for by each code [15], [20], [32], [42]. The pre- and post-INSPYRE versions of both GERMINAL and TRANSURANUS yield almost undistinguishable results.

The evolutions of the fuel central temperature during the first irradiation cycle yielded by the pre-INSPYRE (left) and post-INSPYRE (right) versions of the codes are reported in Figure 9. First, the comparison of the results of the pre-INSPYRE GERMINAL and TRANSURANUS show a difference in the temperature reached at beginning of life and in the qualitative behaviour predicted. In particular, the maximum temperature is calculated for different moments by the two codes: ~1740°C at the beginning of the cycle for GERMINAL against ~ 1800°C at the end of the cycle for TRANSURANUS. This will induce different most critical times for the occurrence of a BPJ. The different evolutions during cycle 1 are mainly ascribed to the different models used for the fuel thermal conductivity, thermal expansion, creep, swelling, as well as fuel relocation. The latter influences strongly the fuel-cladding gap size (reduction) and therefore the gap conductance [15], [32], [43].

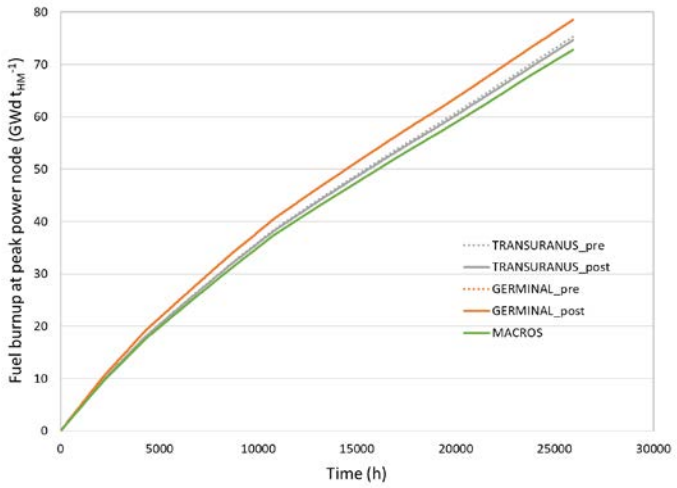

Figure 8: Fuel burnup at the peak power node along the 12 cycles designed for the MYRRHA nominal irradiation yielded by the pre-INSPYRE ("pre") and post-INSPYRE ("post") versions of the codes involved.

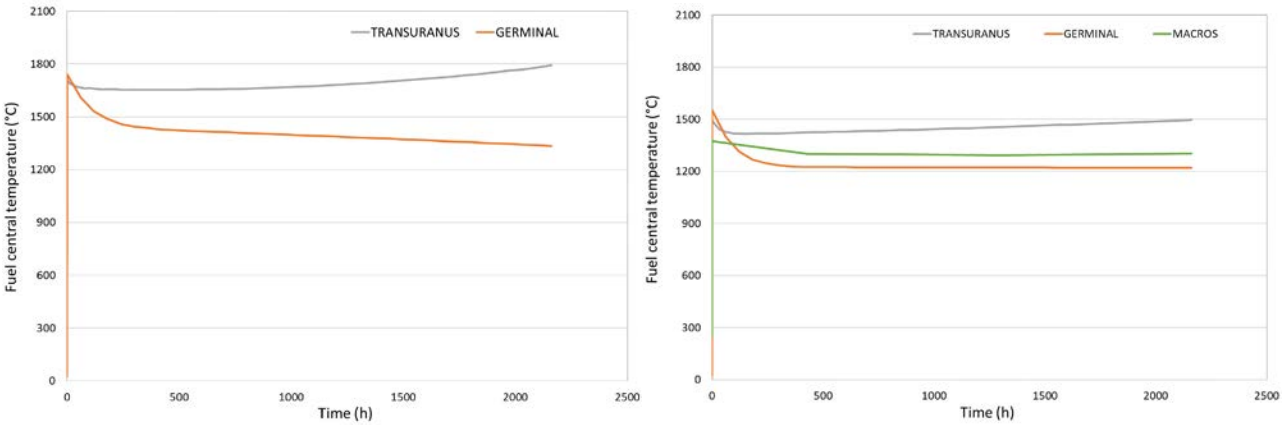

Figure 9: Fuel central temperature at the peak power node during the MYRRHA irradiation cycle 1 yielded by pre-INSPYRE (left) and post-INSPYRE (right) codes.

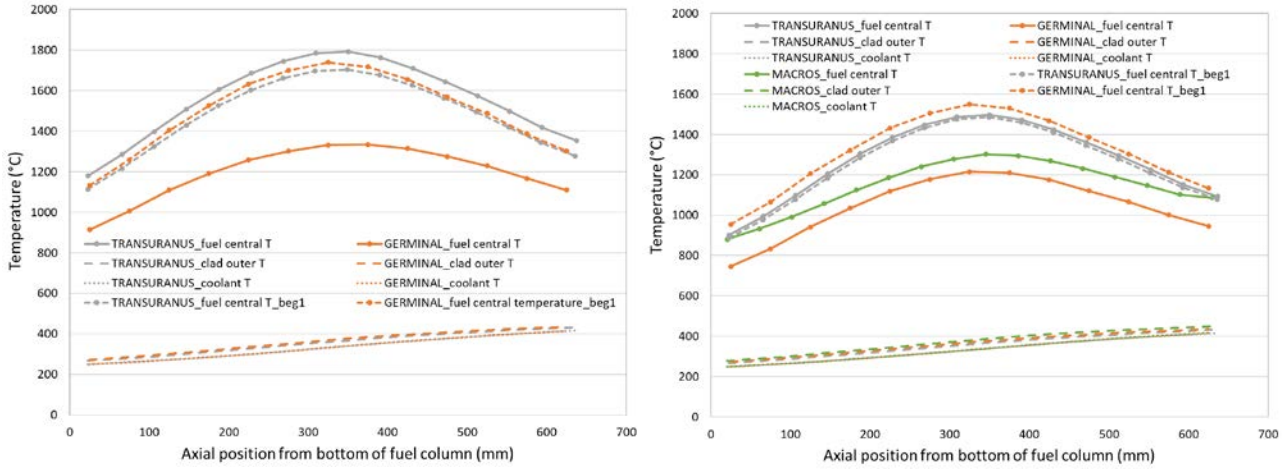

Figure 10: Axial profiles of the fuel central temperature, cladding outer temperature and coolant temperature at the beginning / end of the MYRRHA irradiation cycle 1 yielded by pre-INSPYRE (left) and post-INSPYRE (right) codes.

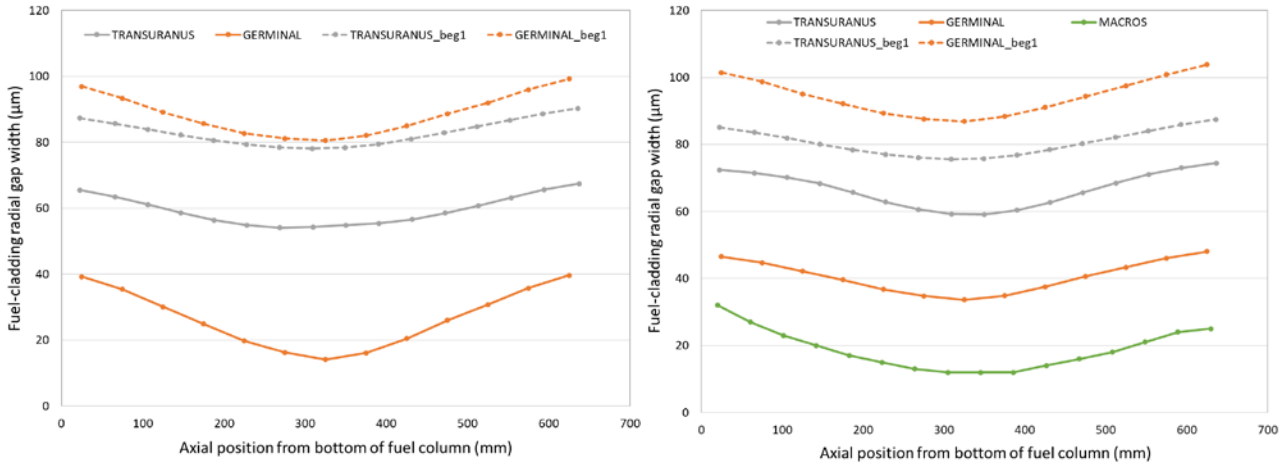

Figure 11: Axial profiles of the fuel-cladding radial gap width at the beginning / end of the MYRRHA irradiation cycle 1 yielded by pre-INSPYRE (left) and post-INSPYRE (right) codes.

In addition, the reduced deviation from fuel stoichiometry (i.e., the increase of the fuel oxygen-to-metal ratio towards 2.00) predicted by GERMINAL at the beginning of irradiation leads to an increase of the thermal conductivity of the fuel material during the first cycle. This, combined to the progressive reduction of the gap size shown in Figure 11 left, induces a decrease of the fuel temperature observed in Figure 9. The results of pre-INSPYRE TRANSURANUS are mainly driven by the fission gas release in the gap during cycle 1 (Figure 14 - left), prevailing over the effect of gap conductance increase due to the gap size reduction. The different approaches adopted in the codes to model the fuel radial relocation also impact the predicted fuel temperatures: the TRANSURANUS model does not allow relocation recovery [43], [44], while the empirical formulation employed by GERMINAL allows a complete accommodation of the relocation [15]. The differences in the temperatures observed, however, are within the range of the experimental uncertainties in the fuel thermal conductivity [38].

The fuel temperature yielded by the post-INSPYRE FPCs are significantly lower than those obtained using the pre-INSPYRE ones. This mainly reflects the effects of the correlations developed in INSPYRE for the MOX thermal conductivity, which is higher at low burnup, and for the thermal expansion [38]–[40], combined with a lower fission gas release (FGR) in the gap at low burnup, inducing a higher gap conductance. GERMINAL yields the maximum fuel central temperature (~ 1550°C) at the beginning of the first cycle, while TRANSURANUS predicts ~ 1500°C at the end of the first cycle. MACROS predicts a lowest fuel central temperature (~ 1370°C) at the beginning of the first cycle, then the temperature is between those obtained by GERMINAL and TRANSURANUS.

The axial profiles of the fuel central temperature, cladding outer temperature and coolant temperatures at the end of the first cycle are reported in Figure 10, while the axial profiles of the fuel-cladding gap size are shown in Figure 11. These figures also include the axial profiles calculated at the beginning of the first cycle by the GERMINAL and TRANSURANUS codes. The pre- and post-INSPYRE codes yield similar profiles for the coolant and cladding outer temperatures, i.e., increasing from the bottom to the top of the fuel column, with a coolant outlet temperature ~ 415°C and an upper cladding outer temperature of ~ 435 – 450°C. The fuel central temperature profiles calculated by all code versions follow the axial profile of the linear power. The axial profiles shown in Figure 10 are consistent with the evolutions in time (for the peak power node) shown in Figure 9. They confirm the identification of two different most critical moments for the BPJ in terms of fuel temperature during the first irradiation cycle by GERMINAL and TRANSURANUS, i.e., the beginning and end of cycle 1, respectively.

As shown in Figure 11, TRANSURANUS and GERMINAL yield different decreases of the fuel-cladding radial gap size during the first irradiation cycle. The smaller gap size calculated by GERMINAL at the end of the first cycle is due to the fuel relocation model, which contributes significantly to the gap closure. In TRANSURANUS, the gap closure is mostly driven by the fuel thermal expansion and the irradiation-induced swelling. The differences between pre- and post-INSPYRE models seem mainly due to the difference in the temperature yielded by the two versions. The gap size reduction is then faster in GERMINAL than in TRANSURANUS, the post-INSPYRE versions providing generally slightly wider gaps.

3.2 Full nominal irradiation

The evolution of the fuel central temperatures calculated by the three codes during the whole irradiation (12 cycles) is shown in Figure 12. It shows clearly that the fuel maximal temperature is not a concern after the first two irradiation cycles. The temperature decreases significantly as irradiation proceeds, reaching ~ 800 – 950°C at the end of irradiation according to pre-INSPYRE code versions and ~ 650 – 870°C according to post-INSPYRE ones, hence respecting a large safety margin towards fuel melting. The pre-INSPYRE version of GERMINAL yields a strong temperature decrease during the first six cycles, when the fuel-cladding gap approaches closure (Figure 20 – left), then the fuel central temperature

increases slightly after gap closure (which occurs at the end of cycle 6, while not predicted by post-INSPYRE GERMINAL). The gap width progressively reduces during irradiation due to the differential fuel and cladding radial deformations (by thermal expansion and swelling). This drives the decrease of the fuel central temperature from the third irradiation cycle on according to TRANSURANUS, not predicting any gap closure. It is important to note the significant differences in the temperature yielded by the pre-INSPYRE versions of GERMINAL and TRANSURANUS, which reaches 800°C during the third and fourth cycles.

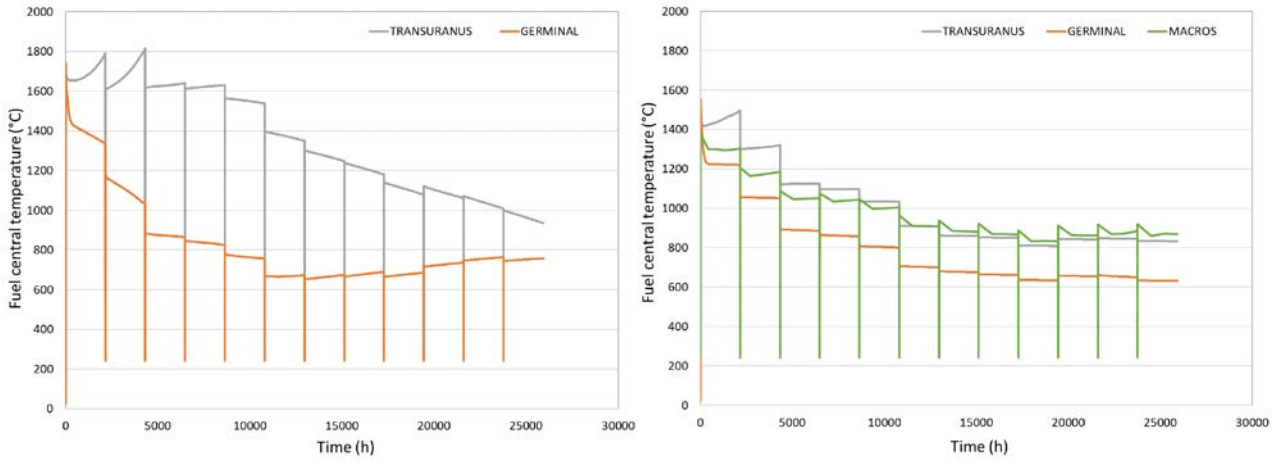

Figure 12: Fuel central temperature at the peak power node during the whole MYRRHA irradiation (12 cycles) yielded by the pre-INSPYRE (left) and post-INSPYRE (right) versions of the codes.

In addition, the fuel temperature regimes yielded by the post-INSPYRE versions of the codes are lower and more stable during the power cycles than those obtained using the pre-INSPYRE ones. Discrepancies among codes are also reduced. The post-INSPYRE version of MACROS predicts the highest fuel central temperature at the end of irradiation, i.e., ~ 870°C, with peculiar temperature peaks caused by power start-ups at the beginning of each cycle. The formation of a fuel central void and of a columnar grain region is not predicted by any of the codes. The fuel temperatures are below the threshold (1800°C [15], [19], [20], [32]) for the fuel central void formation adopted by the current modelling of fuel restructuring in fast reactor conditions.

As already mentioned, the calculated fuel temperatures are sensibly impacted by the evolution of the fuel-cladding gap conductance along the 12 irradiation cycles, determined by the combined effects of progressive gap width reduction (improving the gap conductance during the first half of the irradiation) and fission gas release in the gap (degrading the gap conductance towards the end of irradiation). These effects are particularly shown by GERMINAL, which exhibits a gap conductance peak (~ 30000 W m^{-2} K^{-1}) during cycle 6, i.e., at mid-irradiation, before the decrease due to the progressive FGR in the gap. A lower gap conductance is instead used by MACROS and TRANSURANUS (peaks of ~ 12000 and 5000 W m^{-2} K^{-1}, respectively), driven more by the FGR than by the gap width reduction.

Figure 13 shows the axial profiles of fuel-cladding radial gap width at the end of last irradiation cycle. A closed gap is predicted only by the pre-INSPYRE version of GERMINAL (Figure 13 – left) around the peak power node, while it is still open at the fuel column extremities. The residual gap predicted by the post-INSPYRE version of TRANSURANUS is wider than that obtained using the pre-INSPYRE version of TRANSURANUS. This is due to the correlation for the thermal expansion of MOX fuel developed in INSPYRE [40], as well as to the use of the SCIANTIX module for fission gas behaviour (see Section 2.5) for the fuel swelling instead of the standard empirical correlations available in the code [32], [45], [46]. As for the first cycle (Section 3.1), despite the wider gap, the fuel central temperatures yielded by the post-INSPYRE code versions are lower from the beginning of irradiation, mainly due to a lower FGR in

the gap during the first cycles (Figure 14 – right), which degrades the gap conductance less. The residual gap profile predicted by MACROS is almost flat axially and therefore completely different from the axial power distribution, and exhibits a wider gap at the peak power node.

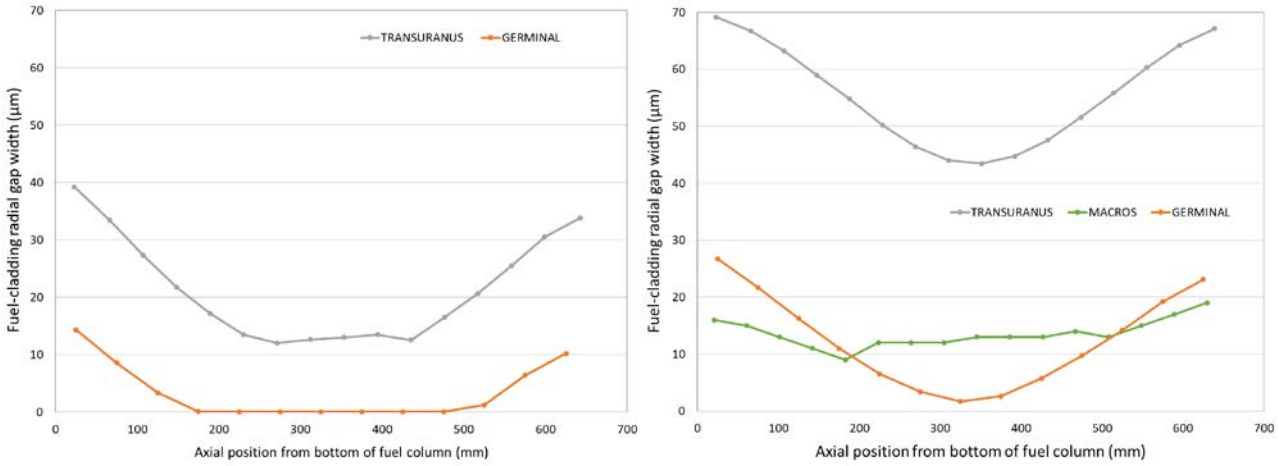

Figure 13: Axial profiles of the fuel-cladding radial gap width at the end of the MYRRHA irradiation cycle 12, as predicted by pre-INSPYRE (left) and post-INSPYRE (right) codes.

Figure 14 shows the substantially different FGR during the MYRRHA nominal irradiation history obtained using the various codes. The pre-INSPYRE version of TRANSURANUS predicts a strong FGR during the first cycle (after an initial incubation period) up to almost 25%. The standard TRANSURANUS model for fission gas behaviour and release includes a saturation threshold for the gas concentration at grain boundaries, above which the release of the excess gas towards the gap is triggered [46]–[48]. This happens during the first cycle, after which the FGR evolution is mostly driven by the fuel temperature regime. Therefore, the FGR increases up to a peak of ~ 43% at the beginning of irradiation while the pin linear power is high. It then decreases due to the reduction in linear power and fuel temperatures, reaching ~ 24% at the end of irradiation. The FGR evolution yielded by the post-INSPYRE TRANSURANUS version, which includes the SCIANTIX module, exhibits an increasing FGR values during each irradiation cycle, as well as sudden gas releases during the MYRRHA inter-cycles, up to an end-of-irradiation value of approximately 50%. The burst releases, occurring mostly during the power shutdowns, are yielded by the model of the micro-cracking of the fuel grain boundaries available in SCIANTIX.

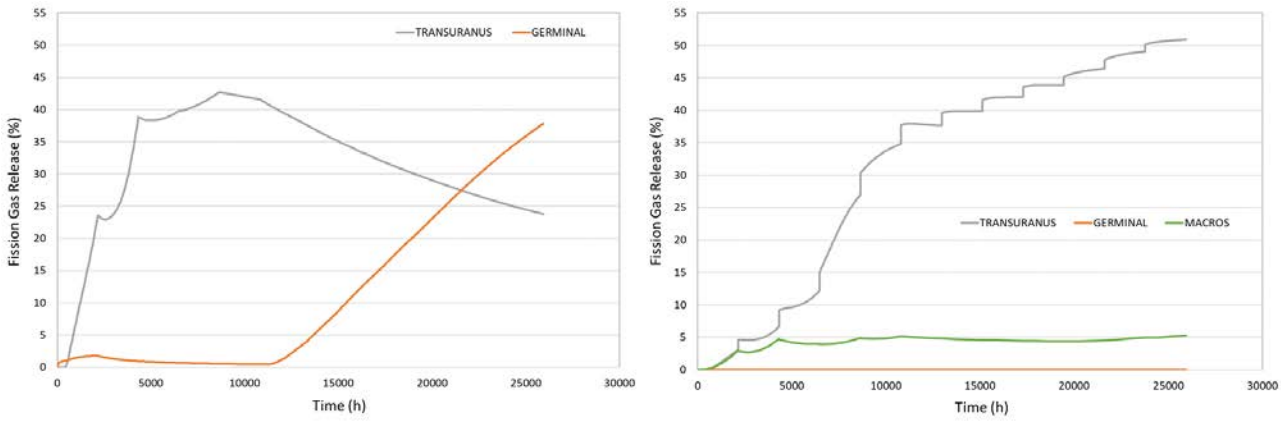

Figure 14: Evolution of the integral fission gas release up to the MYRRHA irradiation cycle 12, as predicted by pre-INSPYRE (left) and post-INSPYRE (right) codes.

The pre-INSPYRE version of GERMINAL yields an opposite FGR behaviour to the one predicted by TRANSURANUS. A long incubation period with a release around 2% is observed until the fifth cycle, when the gas concentration threshold at the grain boundaries is reached. It is then followed by an almost linear increase until the end of the irradiation with a final value of ~ 38%. A null FGR is predicted by the post-INSPYRE version of GERMINAL, which includes the SCIANTIX fission gas behaviour module. This is due to a temperature threshold governing the FGR in the fuel-cladding gap, which is not reached due to the low temperature calculated. A lower FGR is anyway expected from post-INSPYRE codes considering the lower fuel temperature regimes obtained, as seen in Figure 12.

4 RESULTS OF THE SIMULATION OF THE MYRRHA FUEL PIN IN A TRANSIENT SCENARIO

This Section focuses on the impact of a potential BPJ transient occurring during the first or the twelfth cycle on the MYRRHA hottest pin considered by the codes. Based on the results presented in Section 3, the first cycle is identified as the most critical moment during the MYRRHA nominal irradiation history in terms of maximal fuel temperature for the occurrence of a BPJ transient. The end of the twelfth cycle is the worst case in terms of fuel-cladding mechanical interaction and potential cladding plasticity caused by gap closure.

4.1 Beam power jump during the first cycle

The most relevant impact of a BPJ occurring at cycle 1 (when the MYRRHA power is the highest) is the sudden increase of the fuel central temperature, as shown in Figures 15 and 16. Both the pre- and post-INSPYRE versions of TRANSURANUS yield the highest fuel temperature at the axial peak power node for a BPJ occurring at the end of the first cycle. These temperatures are equal to ~ 2510°C and ~ 2370°C, respectively. TRANSURANUS also yields the largest increase of the fuel central temperature, ~ 800°C against ~ 500°C for GERMINAL and MACROS. GERMINAL predicts the worst BPJ scenario at the beginning of the first cycle, and not at the end.

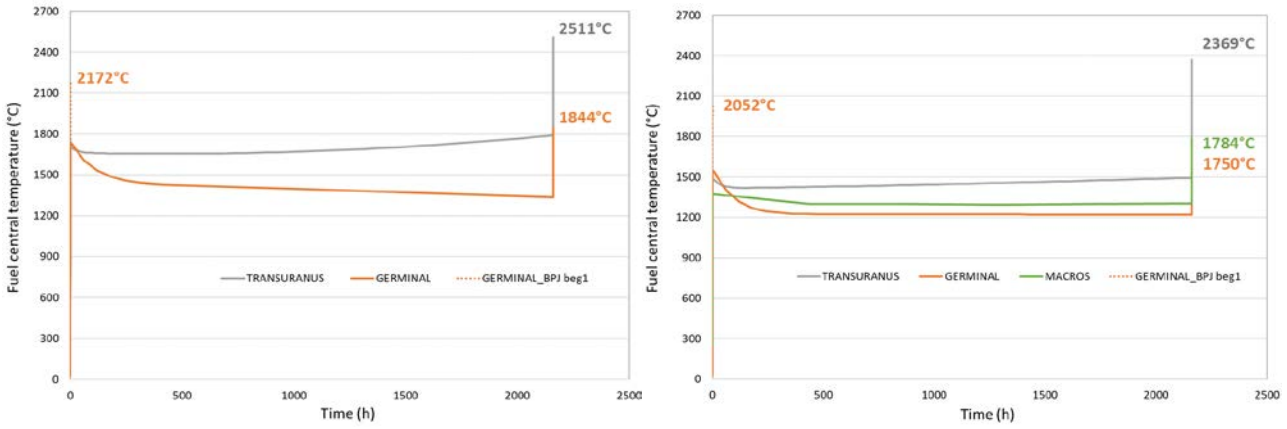

Figure 15: Evolution of the fuel central temperature at the peak power node up to the BPJ during the MYRRHA irradiation cycle 1, as predicted by pre-INSPYRE (left) and post-INSPYRE (right) codes.

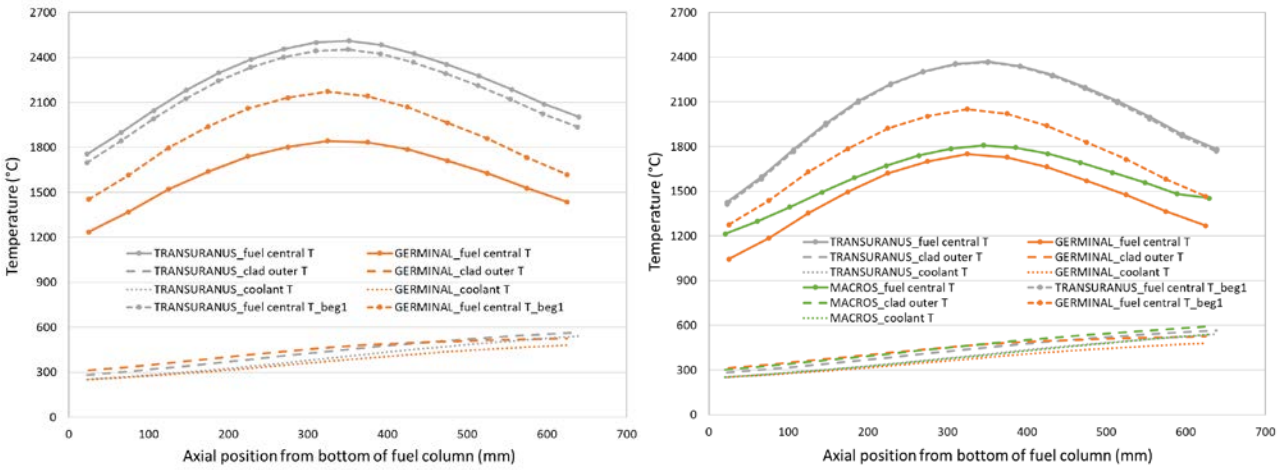

Figure 16: Axial profiles of the fuel central temperature, cladding outer temperature and coolant temperature after the BPJ during the MYRRHA irradiation cycle 1, as predicted by pre-INSPYRE (left) and post-INSPYRE (right) codes.

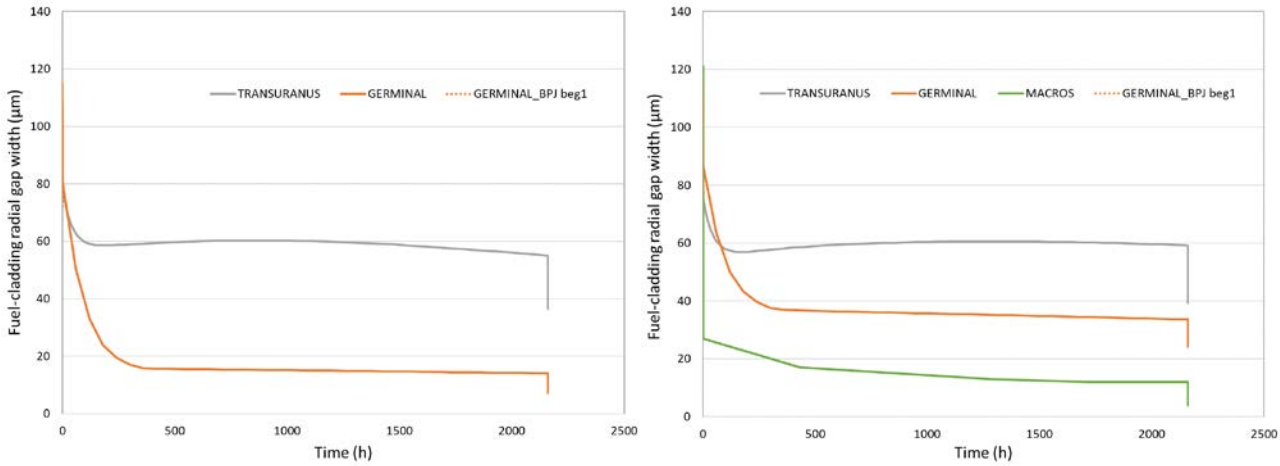

Figure 17: Evolution of the fuel-cladding radial gap width at the peak power node up to the BPJ during the MYRRHA irradiation cycle 1, as predicted by pre-INSPYRE (left) and post-INSPYRE (right) codes.

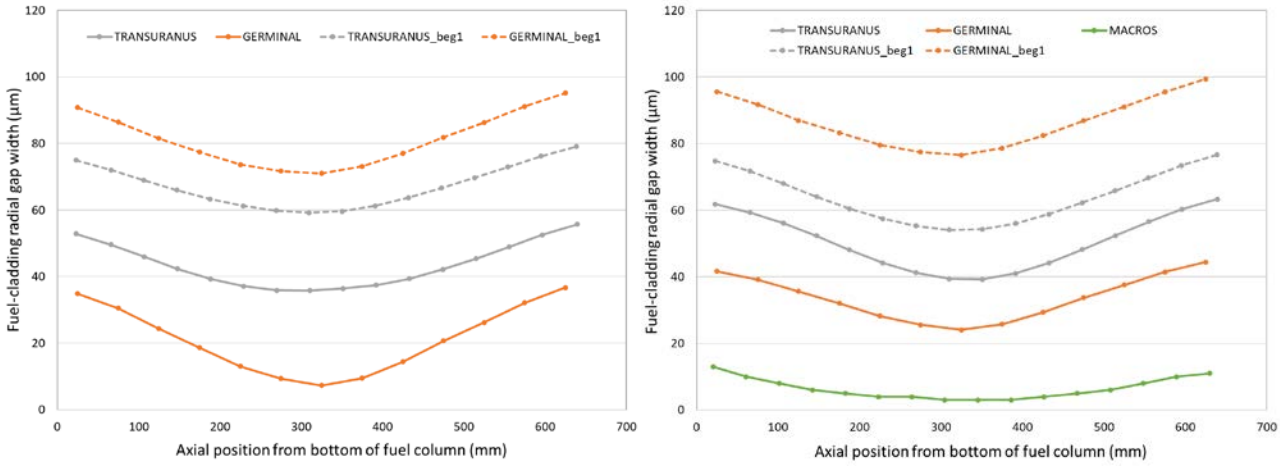

Figure 18: Axial profiles of the fuel-cladding radial gap width after the BPJ during the MYRRHA irradiation cycle 1, as predicted by pre-INSPYRE (left) and post-INSPYRE (right) codes.

The highest fuel temperature predicted by the pre-INSPYRE version of GERMINAL is ~ 2170°C at the peak power node. The post-INSPYRE calculations yield lower fuel temperatures due to the new correlation for the MOX thermal conductivity, the effect on the gap conductance of the new correlation for the MOX thermal expansion and the treatment of fission gas behaviour and release by the SCIANTIX module. The calculations using the post-INSPYRE version of MACROS calculations yield a fuel maximal temperature after the BPJ at the end of the first cycle of ~ 1800°C.

The axial profiles of cladding outer temperature and coolant temperature calculated are similar between the three codes and between the pre- and post-INSPYRE versions. They yield ~ 540°C for the coolant outlet temperature and 565 – 590°C for the cladding outer temperature at the top of the column, apart from GERMINAL that yields lower values (~ 480°C and ~ 525°C, respectively). The very fast increase of the cladding temperature during a BPJ transient causes a step-wise cladding radial deformation due to thermal expansion.

Figures 17 and 18 show the evolution in time and axial profiles of the residual fuel-cladding gap width. It can be seen that none of the codes predicts a gap closure even after the BPJ in the first cycle, despite the sudden thermal expansion of the fuel pellets and the sudden decrease of the gap width. Gap closure is approached in the results of the pre-INSPYRE version of GERMINAL (~ 7 μm) and the post-INSPYRE version of MACROS (~ 3 μm), while a significant residual gap still remains (~ 40 μm) according to TRANSURANUS. The higher temperature at the beginning of the BPJ yielded by TRANSURANUS, compared to GERMINAL, leads to a higher fuel maximal temperature during the transient. Generally, wider gaps are predicted by the post-INSPYRE versions of GERMINAL and TRANSURANUS, mostly due to the lower thermal expansion of a colder fuel.

4.2 Beam Power Jump during the 12th cycle

Figures 19, 20 and 21 show the evolution of the fuel central temperature, the fuel-cladding radial gap width and the Von Mises equivalent stresses at the peak power node until and during the BPJ at the end of the 12th irradiation cycle.

The highest fuel central temperature after the BPJ at the end of life is yielded by the pre-INSPYRE version of TRANSURANUS and approaches 1400°C. It is therefore well below the fuel central temperature resulting from the BPJ in the first cycle (Figure 15) due to the reduced nominal fuel temperatures caused by the lower linear power towards the end of irradiation. The BPJ occurring at the end of the MYRRHA irradiation still causes the fuel temperatures to increase sharply, but it is not of concern for the safety margin in terms of fuel melting. In terms of axial profiles, the fuel central temperature from the calculations using post-INSPYRE versions are close to the axial linear power distribution, while the temperature yielded by pre-INSPYRE versions is more determined by the fuel-cladding gap width. In particular, GERMINAL provides higher temperatures at the extremities of the fuel column, where the gap is still open, than at the peak power node where the gap is closed.

The residual width of the fuel-cladding gap suddenly decreases due to the fuel thermal expansion caused by the fast BPJ transient. While the gap is already closed from the end of cycle 6 according to the pre-INSPYRE version of GERMINAL, the gap closes just due to the final BPJ according to post-INSPYRE GERMINAL. The gap according to GERMINAL approaches closure also at the fuel column extremities after the BPJ occurrence at the end of irradiation. The JOG formation observed at the fuel-cladding interface in fast reactor fuel pins at sufficiently high burnup [49]–[51] is not predicted by GERMINAL, even at the end of the MYRRHA irradiation, since the final fuel burnup is just below the threshold value in the model for the JOG evolution to start. The re-opening of the fuel-cladding gap due to JOG formation is hence not predicted by GERMINAL, while this was the case for the ASTRID case study [52].

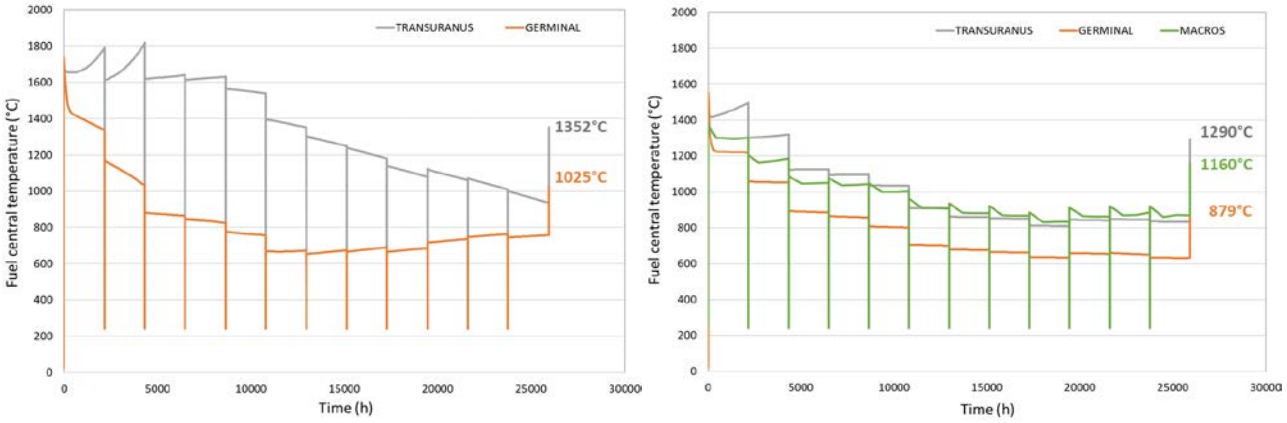

Figure 19: Fuel central temperature at the peak power node until the BPJ at the end of the 12th irradiation cycle yielded by pre-INSPYRE (left) and post-INSPYRE (right) codes.

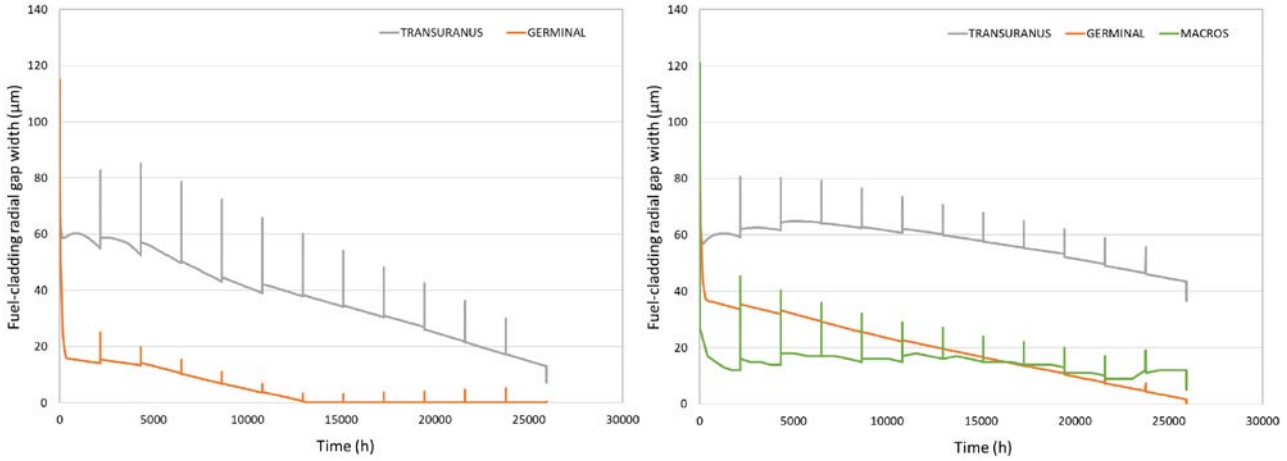

Figure 20: Fuel-cladding radial gap width at the peak power node until the BPJ at the end of the 12th irradiation cycle yielded by pre-INSPYRE (left) and post-INSPYRE (right) codes.

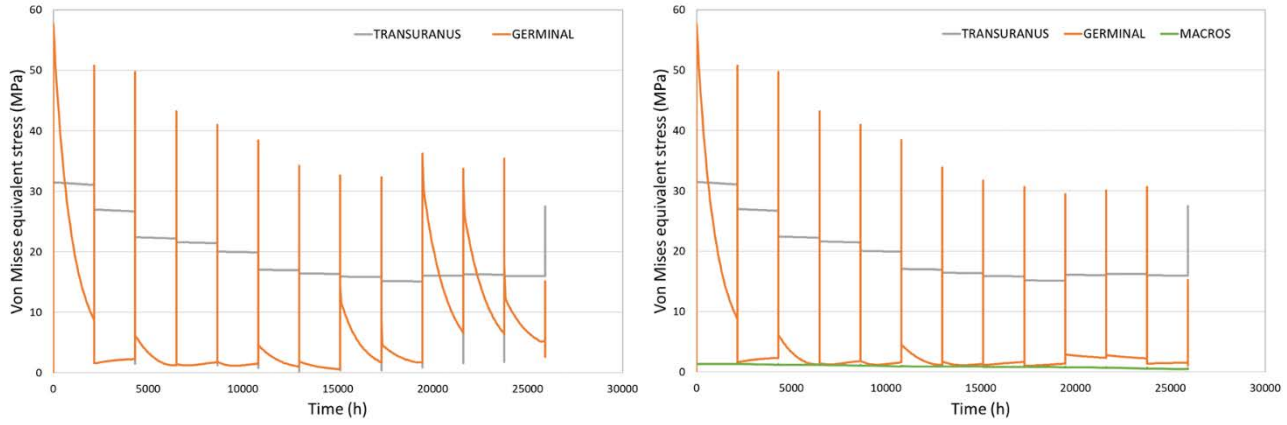

Figure 21: Von Mises equivalent stresses in the cladding at the peak power node until the BPJ at the end of the 12th irradiation cycle yielded by pre-INSPYRE (left) and post-INSPYRE (right) codes.

The gap never closes according to both pre- and post-INSPYRE versions of TRANSURANUS and MACROS. TRANSURANUS yields the wider residual gap size, which is sensibly different between pre- and post-INSPYRE calculations (minimum ~ 7 µm and ~ 35 µm, respectively). The gap size calculated by MACROS remains quite constant after the strongest gap reduction calculated after the first power rise at reactor start-up. All codes predict gap re-openings during the inter-cycles, when a batch is moved from the previous to the next irradiation position in the MYRRHA core (Figure 3).

Finally, the occurrence of a BPJ transient causes a sudden increase of the stress levels in the cladding yielded by the codes, as shown in Figure 21 for the BPJ during the 12th cycle. All code versions yield a progressive decrease of the cladding stress levels during the MYRRHA nominal irradiation, mainly due to irradiation-induced creep contributing to cladding relaxation. Both the pre- and post-INSPYRE versions of GERMINAL yield spikes of stress levels during the irradiation inter-cycles. Then, the Von Mises equivalent stresses reach ~ 15 MPa, 0.64 MPa and 27.5 MPa due to the final BPJ according to GERMINAL, MACROS and TRANSURANUS, respectively. Actually, the codes provide higher equivalent stress values during the first irradiation cycle, hence the maximum stress values are yielded after the BPJ occurring at cycle 1. These values are around 50 MPa according to TRANSURANUS and 73 MPa according to GERMINAL. In terms of local values, MACROS provides the highest (hoop) stress (at the inner cladding surface), equal to ~ 101 MPa, despite the lowest Von Mises equivalent stress (~ 1.88 MPa) related to the "soft" contact assumed by MACROS for the fuel-cladding mechanical interaction.

4.3 Compliance with MYRRHA design limits

For the margin to fuel melting, the most critical scenario corresponds to the BPJ occurring during the first cycle and the minimum margin is predicted by the pre-INSPYRE version of TRANSURANUS, ~ 100°C (maximum fuel central temperature of ~ 2510°C at the axial peak power node reached with a BPJ at the end of the first cycle). It must be noted, however, that the design limit is conservatively set at 2600°C, but the fuel melting (solidus) temperature is actually higher even accounting for the 30%Pu content in as-fabricated MYRRHA fuel pellets and burnup of about 75 GWd t_{HM}^{-1} at the end of life [38], [39]. Hence, despite this conservative design limit, no failure related to fuel melting is predicted in the MYRRHA conditions considered. The post-INSPYRE codes provide even lower temperatures for the MYRRHA fuel, showing higher safety.

The beam power jump at the end of the twelfth cycle is potentially of concern in terms of fuel-cladding mechanical interaction and cladding integrity, since this BPJ occurs when the residual gap size is the lowest, according to the post-INSPYRE version of MACROS and the pre-INSPYRE version of TRANSURANUS, or even when the gap is closed, according to pre-INSPYRE GERMINAL. Concerning the design limit on the cladding plasticity, first an equivalent (Von Mises) stress can be compared with the cladding yield stress. Since the yield stress decreases with temperature, a minimum value of 400 MPa for the yield stress can be conservatively adopted for the MYRRHA DIN 1.4970 cladding at the highest operative temperature reached (~ 600°C), consistently with what reported by [53]–[55]. The conservative value adopted should also account for the irradiation effect on the yield stress of DIN 1.4970 cladding steels, which should slightly increase under fast neutron fluence [56], [57], hence extending the elastic regime. Since the equivalent stresses in the cladding are well below the yield stress of the cladding steel, according to the calculations of all codes, any cladding plasticity is prevented even considering the occurrence of BPJ transients. The design limit of maximum 0.5% cladding plasticity is consequently respected.

5 CONCLUSIONS AND FUTURE DEVELOPMENTS

This Deliverable presents the results of the simulation of both nominal irradiation of MYRRHA MOX-fuelled driver pins and the potential occurrence of Beam Power Jump (over-power) transient scenarios in beginning-of-life and end-of-life conditions, using the European fuel performance codes GERMINAL, MACROS and TRANSURANUS.

The analysis of the MYRRHA fuel and cladding performance under irradiation focused on the hottest pin to provide conservative predictions about the thermal-mechanical behaviour under irradiation. The activity involved the application of the reference code versions ("pre-INSPYRE"), existing prior to the INSPYRE Project, and of "post-INSPYRE" codes equipped with the novel INSPYRE models for MOX fuel properties. These modelling advances concern the thermal properties (thermal conductivity, melting temperature), mechanical properties (thermal expansion, Young's modulus) and the mechanistic treatment of fission gas behaviour and release from MOX fuels (implemented in the SCIANTIX module coupled to GERMINAL and TRANSURANUS).

The simulation results from the pre-INSPYRE and post-INSPYRE versions are compared to assess the predictive capabilities of the fuel performance codes on ADS-LBE fast reactor fuel and to evaluate the impact of the models for MOX fuel properties developed in INSPYRE on the MYRRHA pin integral behaviour. The outcomes of these simulations, which are the first openly available, enabled the evaluation of the safety limits of the current MYRRHA fuel design, i.e., the margin to fuel melting and the cladding plasticity in representative operational conditions. Results show that adequate margins are respected during the whole MYRRHA driver irradiation to avoid fuel melting and ensure cladding integrity, even in the case of the hottest fuel pin and of BPJ transients.

The results presented here constitute a solid basis for further analyses and allow us to identify the modelling developments needed to improve the code capabilities for the simulation of fast reactor conditions and LBE-cooled pins. In particular:

- Considering a partial accommodation of fuel relocation would help in harmonizing the simulations of residual fuel-cladding gap size and improve the evaluation of the pellet-cladding mechanical interaction after gap closure, providing proper estimations of the cladding stress levels accounting for the fuel contact pressure. Currently, the TRANSURANUS code does not consider any relocation recovery, while GERMINAL allows for a complete radial accommodation of fuel fragments. MACROS already accounts for a partial recovery of fuel relocation, resulting in a "soft" interaction between fuel and cladding when gap closure is reached.
- A model for the normal grain growth of fast reactor fuels is still needed and would improve the simulation results of inert gas behaviour and release. In addition, the specific MYRRHA irradiation conditions (fast neutron fluxes but low linear power and fuel temperatures compared to typical FR ones) call for a dedicated modelling of e.g., parameters of the gas diffusion models and fuel microstructure evolution.
- A proper model for LBE coolant corrosion on the outer surface of austenitic stainless steel claddings, disregarded in this work, should be taken into account. This should have a significant impact on the heat exchange with the coolant. An outer oxide layer on the cladding would influence the pin temperature, as well as the cladding structural integrity. Additionally, to limit corrosion issues on the MYRRHA cladding from flowing LBE coolant, specific design limits should be set on the maximal cladding temperature relevant for normal operation conditions (corrosion effects are not active on the fast time scales of power transients).

The MYRRHA fuel element is now being investigated in the PATRICIA European H2020 Project [58], devoted to feasibility studies of the application of the MYRRHA facility for transmutation purposes, i.e., employing Am-bearing mixed oxide fuels. The MYRRHA pin performance will be analysed in sub-critical and potentially critical core configurations, considering also accidental irradiation scenarios, in particular beam power jumps for the sub-critical core and reactivity-initiated accidents for the critical core.

REFERENCES

[1] GIF (Generation IV International Forum), "Technology Roadmap Update for Generation IV Nuclear Energy Systems", 2014. [Online]. Available: https://www.gen-4.org/gif/upload/docs/application/pdf/2014-03/gif-tru2014.pdf.

[2] ESNII Task Force, "Demonstration Programme for Fast Neutron Reactors", Concept Paper, pp. 1–36, 2010.

[3] T. Beck *et al.*, "Conceptual design of ASTRID fuel sub-assemblies", *Nucl. Eng. Des.*, vol. 315, pp. 51–60, 2017.

[4] G. Grasso *et al.*, "The core design of ALFRED, a demonstrator for the European lead-cooled reactors", *Nucl. Eng. Des.*, vol. 278, pp. 287–301, 2014.

[5] H. A. Abderrahim *et al.*, "MYRRHA accelerator driven system programme: Recent progress and perspectives", *Nucl. Power Eng.*, no. 2, pp. 29–41, 2019.

[6] R. Stainsby *et al.*, "Gas cooled fast reactor research in Europe", *Nucl. Eng. Des.*, vol. 241, pp. 3481–3489, 2011.

[7] P. Pónya and S. Czifrus, "Core optimisation issues of MOX fueled ALLEGRO reactor", *Ann. Nucl. Energy*, vol. 108, pp. 188–197, 2017.

[8] H. A. Abderrahim *et al.*, "Partitioning and transmutation contribution of MYRRHA to an EU strategy for HLW management and main achievements of MYRRHA related FP7 and H2020 projects: MYRTE, MARISA, MAXSIMA, SEARCH, MAX, FREYA, ARCAS", *Nucl. Sci. Technol.*, vol. 33, pp. 1–8, 2020.

[9] I. L. Pioro, *Handbook of Generation IV Nuclear Reactors*, Elsevier Ltd., Woodhead Publishing, 2016.

[10] P. Van Uffelen and M. Suzuki, "Oxide fuel performance modeling and simulations", in: *Comprehensive Nuclear Materials*, vol. 3, pp. 535-577, Elsevier Inc., 2012.

[11] Y. Guerin, "Fuel Performance of Fast Spectrum Oxide Fuel", in: *Comprehensive Nuclear Materials (Second Edition)*, vol. 2, pp. 72-105, Elsevier Inc., 2020.

[12] A. E. Waltar *et al.*, *Fast Spectrum Reactors*, Springer, 2012.

[13] EERA-JPNM, "INSPYRE - Investigations Supporting MOX Fuel Licensing in ESNII Prototype Reactors", 2017. [Online]. Available: *http://www.eera-jpnm.eu/inspyre/*.

[14] D. De Bruyn *et al.*, "Recent Developments in the Design of the Belgian MYRRHA ADS Facility", in: *2016 International Congress on Advances in Nuclear Power Plants (ICAPP'16)*, 17-20 April 2016, San Francisco, California, USA, 2016.

[15] M. Lainet *et al.*, "GERMINAL, a fuel performance code of the PLEIADES platform to simulate the in-pile behaviour of mixed oxide fuel pins for sodium-cooled fast reactors", *J. Nucl. Mater.*, vol. 516, pp. 30–53, 2019.

[16] B. Michel *et al.*, "Two fuel performance codes of the PLEIADES platform: ALCYONE and GERMINAL", in: *Nuclear Power Plant Design and Analysis Codes - Development, Validation and Application*, Chap. 9, pp. 207-233, Elsevier, 2021.

[17] A. Magni *et al.*, "The TRANSURANUS fuel performance code", in: *Nuclear Power Plant Design and Analysis Codes - Development, Validation and Application*, Chap. 8, pp. 161–205, Elsevier, 2021.

[18] P. Van Uffelen *et al.*, "Incorporation and verification of models and properties in fuel performance codes", INSPYRE Deliverable D7.5, 2020.

[19] S. E. Lemehov *et al.*, "MACROS benchmark calculations and analysis of fission gas release in MOX with high content of plutonium", *Prog. Nucl. Energy*, vol. 57, pp. 117–124, 2012.

[20] S. E. Lemehov *et al.*, "Predicting thermo-mechanical behaviour of high minor actinide content composite oxide fuel in a dedicated transmutation facility", *J. Nucl. Mater.*, vol. 416, no. 1–2, pp. 179–191, 2011.

[21] MYRRHA Consortium, "MYRRHA Project website", 2022. [Online]. Available: *https://www.myrrha.be/*.

[22] Sustainable Nuclear Energy Technology Platform, "ESNII - SNETP website", 2022. [Online]. Available: https://snetp.eu/.

[23] H. A. Abderrahim *et al.*, "MYRRHA - A multi-purpose fast spectrum research reactor", *Energy Convers. Manag.*, vol. 63, pp. 4–10, 2012.

[24] H. A. Abderrahim *et al.*, "Fuel design for the experimental ADS MYRRHA", in: *Technical Meeting on use of LEU in ADS*, October 2005, IAEA, Vienna, Austria, 2005.

[25] D. De Bruyn *et al.*, "The MYRRHA ADS project in Belgium enters the Front End Engineering Phase", *Phys. Procedia*, vol. 66, pp. 75–84, 2015.

[26] R. Fernandez *et al.*, "The Evolution of the Primary System Design of the MYRRHA Facility", in: *FR17 - IAEA International Conference on Fast Reactors and Related Fuel Cycles: Next Generation Nuclear Systems for Sustainable Development*, June 2017, Yekaterinburg, Russia, 2017.

[27] A. Toti *et al.*, "Coupled system thermal-hydraulic/CFD analysis of a protected loss of flow transient in the MYRRHA reactor", *Ann. Nucl. Energy*, vol. 118, pp. 199–211, 2018.

[28] G. Van Den Eynde *et al.*, "An updated core design for the multi-purpose irradiation facility MYRRHA", *J. Nucl. Sci. Technol.*, vol. 52, no. 7–8, pp. 1053–1057, 2015.

[29] P. Romojaro *et al.*, "Nuclear data sensitivity and uncertainty analysis of effective neutron multiplication factor in various MYRRHA core configurations", *Ann. Nucl. Energy*, vol. 101, pp. 330–338, 2017.

[30] K. Van Tichelen *et al.*, "Advanced Liquid-Metal Thermal-Hydraulic Research for MYRRHA", *Nucl. Technol.*, vol. 206, no. 2, pp. 150–163, 2019.

[31] B. Boer, "Analysis of MYRRHA fuel performance in a Beam Power Jump scenario", INSPYRE internal document, 2019.

[32] European Commission, *TRANSURANUS Handbook*, Joint Research Centre, Karlsruhe, Germany, 2020.

[33] OECD/NEA, *Handbook on Lead-bismuth Eutectic Alloy and Lead Properties, Materials Compatibility, Thermal-hydraulics and Technologies*, 2007 Edition, Technical Report NEA No. 6195, 2007.

[34] Y. Philipponneau, "Thermal conductivity of (U, Pu)O_{2-x} mixed oxide fuel", *J. Nucl. Mater.*, vol. 188, no. C, pp. 194–197, 1992.

[35] OECD/NEA, *Handbook on Lead-bismuth Eutectic Alloy and Lead Properties, Materials Compatibility, Thermal- hydraulics and Technologies*, 2015 Edition, Technical Report NEA No. 7268, 2015.

[36] V. Sobolev, "Properties of Liquid Metal Coolants", in: *Comprehensive Nuclear Materials,* vol. 2, pp. 373–392, Elsevier Inc., 2012.

[37] P. A. Ushakov *et al.*, "Heat transfer to liquid metals in regular arrays of fuel elements", *High Temp.*, vol. 15, no. 5, pp. 868–873, 1977.

[38] A. Magni *et al.*, "Modelling and assessment of thermal conductivity and melting behaviour of MOX fuel for fast reactor applications", *J. Nucl. Mater.*, vol. 541, 152410, 2020.

[39] A. Magni *et al.*, "Report on the improved models of melting temperature and thermal conductivity for MOX fuels and JOG", INSPYRE Deliverable D6.2, version 2, 2020.

[40] S. E. Lemehov, "New correlations of thermal expansion and Young's modulus based on existing literature and new data", INSPYRE Deliverable D6.3, 2020.

[41] D. Pizzocri *et al.*, "SCIANTIX: A new open source multi-scale code for fission gas behaviour modelling designed for nuclear fuel performance codes", *J. Nucl. Mater.*, vol. 532, 152042, 2020.

[42] K. Lassmann *et al.*, "Extension of the TRANSURANUS burnup model to heavy water reactor conditions", *J. Nucl. Mater.*, vol. 255, no. 2–3, pp. 222–233, 1998.

[43] K. Lassmann and F. Hohlefeld, "The revised URGAP model to describe the gap conductance between fuel and cladding", *Nucl. Eng. Des.*, vol. 103, no. 2, pp. 215–221, 1987.

[44] T. Preusser and K. Lassmann, "Current Status of the Transient Integral Fuel Element Performance Code URANUS", in: SMiRT, vol. 7, 22-26 August 1983, Chicago, USA, 1983.

[45] P. Van Uffelen *et al.*, "Multiscale modelling for the fission gas behaviour in the TRANSURANUS Code", *Nucl. Eng. Technol.*, vol. 43, no. 6, pp. 477–488, 2011.

[46] G. Pastore *et al.*, "Physics-based modelling of fission gas swelling and release in UO_2 applied to integral fuel rod analysis", *Nucl. Eng. Des.*, vol. 256, pp. 75–86, 2013.

[47] G. Pastore, "Modelling of Fission Gas Swelling and Release in Oxide Nuclear Fuel and Application to the TRANSURANUS Code", PhD Thesis, Politecnico di Milano, Italy, 2012.

[48] G. Pastore *et al.*, "Modeling of transient fission gas behavior in oxide fuel and application to the BISON code", in: *Proc. Enlarg. Halden Program. Group Meeting*, Roros, Norway, 2014.

[49] F. Cappia *et al.*, "Electron microscopy characterization of fast reactor MOX Joint Oxyde-Gaine (JOG)", *J. Nucl. Mater.*, vol. 531, 151964, 2020.

[50] R. J. Parrish *et al.*, "Comparison of the radial effects of burnup on fast reactor MOX fuel microstructure and solid fission products", *J. Nucl. Mater.*, vol. 531, 152003, 2020.

[51] M. Teague *et al.*, "Microstructural characterization of high burn-up mixed oxide fast reactor fuel", *J. Nucl. Mater.*, vol. 441, no. 1–3, pp. 267–273, 2013.

[52] A. Magni *et al.*, "Application of the SCIANTIX fission gas behaviour module to the integral pin performance in sodium fast reactor irradiation conditions", *Nucl. Eng. Technol.*, vol. 54, pp. 2395–2407, 2022.

[53] S. Holmstrom *et al.*, "Determination of high temperature material properties of 15-15Ti steel by small specimen techniques", Report EUR 28746 EN, Publications Office of the European Union, Luxembourg, 2017.

[54] A. Strafella *et al.*, "Creep behaviour of 15-15Ti(Si) austenitic steel in air and in liquid lead at 550°C", *Procedia Struct. Integr.*, vol. 3, pp. 484–497, 2017.

[55] A. Strafella *et al.*, "15-15Ti(Si) austenitic steel: creep behaviour in hostile environment", *Frat. ed Integrità Strutt.*, vol. 42, pp. 352–365, 2017.

[56] J. R. Weir *et al.*, "Irradiation behavior of cladding and structural materials", Report ORNL-TM-2258, 1968.

[57] M. Nakatsuka, "Mechanical Properties of Neutron Irradiated Fuel Cladding Tubes", *J. Nucl. Sci. Technol.*, vol. 28, no. 4, pp. 356–368, 1991.

[58] European Union's Horizon 2020 Research and Innovation programme, "PATRICIA - Partitioning And Transmuter Research Initiative in a Collaborative Innovation Action", 2020. [Online]. Available: *https://patricia-h2020.eu/*.